Technology and Health Care 18 (2010) 1–17
DOI 10.3233/THC-2010-0565
IOS Press

A framework for human spine imaging using a freehand 3D ultrasound system

Ketut E. Purnama[a,b], Michael. H. F. Wilkinson[c], Albert G. Veldhuizen[e], Peter. M. A. van Ooijen[f], Jaap Lubbers[b], Johannes G.M. Burgerhof[g], Tri A. Sardjono[a,b] and Gijbertus J. Verkerke[b,d,*]

[a]*Department of Electrical Engineering, Sepuluh Nopember Institute of Technology, Surabaya, Indonesia*
[b]*Department of Biomedical Engineering, University Medical Center Groningen, University of Groningen, The Netherlands*
[c]*Institute for Mathematics and Computing Science, University of Groningen, The Netherlands*
[d]*Department of Biomedical Engineering, University of Twente, The Netherlands*
[e]*Department of Orthopaedic Surgery, University Medical Center Groningen, University of Groningen, The Netherlands*
[f]*Department of Radiology, University Medical Center Groningen, University of Groningen, The Netherlands*
[g]*Department of Epidemiology and Bioinformatics, University Medical Center Groningen, University of Groningen, The Netherlands*

Received 23 August 2009
Revised /Accepted 21 September 2009

Abstract. The use of 3D ultrasound imaging to follow the progression of scoliosis, i.e., a 3D deformation of the spine, is described. Unlike other current examination modalities, in particular based on X-ray, its non-detrimental effect enables it to be used frequently to follow the progression of scoliosis which sometimes may develop rapidly. Furthermore, 3D ultrasound imaging provides information in 3D directly in contrast to projection methods.

This paper describes a feasibility study of an ultrasound system to provide a 3D image of the human spine, and presents a framework of procedures to perform this task. The framework consist of an ultrasound image acquisition procedure to image a large part of the human spine by means of a freehand 3D ultrasound system and a volume reconstruction procedure which was performed in four stages: bin-filling, hole-filling, volume segment alignment, and volume segment compounding.

The overall results of the procedures in this framework show that imaging of the human spine using ultrasound is feasible. Vertebral parts such as the transverse processes, laminae, superior articular processes, and spinous process of the vertebrae appear as clouds of voxels having intensities higher than the surrounding voxels. In sagittal slices, a string of transverse processes appears representing the curvature of the spine. In the bin-filling stage the estimated mean absolute noise level of a single measurement of a single voxel was determined. Our comparative study for the hole-filling methods based on rank sum statistics proved that the pixel nearest neighbour (PNN) method with variable radius and with the proposed olympic operation is the best method. Its mean absolute grey value error was less in magnitude than the noise level of a single measurement.

Keywords: Human spine, scoliosis, ultrasound image acquisition, freehand 3D ultrasound system, bin-filling, hole-filling, volume segment alignment, volume segment compounding

*Address for correspondence: G.J. Verkerke, Department of Biomedical Engineering, University Medical Center Groningen, University of Groningen, Antonious Deusinglaan 1, 9713 AV Groningen, The Netherlands. Tel.: +31 50 363 2463; Fax: +31 50 363 3139; E-mail: g.j.verkerke@med.umcg.nl.

Fig. 1. Posterior-Anterior (left) and lateral (right) X-ray images of a human scoliotic spine.

1. Introduction

Scoliosis is a three-dimensional deformity of the spinal column and is usually characterized by a lateral deviation of the spine, accompanied by an axial rotation of the vertebrae. The progression of scoliosis treatment is different among patients. Hence, for optimal treatment the progression needs to be examined frequently by the orthopaedic surgeon. So far, the most common procedure to evaluate the progression is by taking bi-planar radiographs (X-ray images), lateral and posterior-anterior images (Fig. 1). Out of the images, the necessary information in the scoliosis assessment, the spinal curvature and the axial rotation of the vertebrae, are derived.

Following scoliosis progression based on X-rays has two major drawbacks. The first drawback is that taking X-ray images introduces detrimental radiation exposure. For instance, women who were exposed to multiple diagnostic X-rays during childhood or adolescence were found to have an increased risk of having breast cancer [5]. This limits the use of X-rays to once or twice annually. On the other hand, since the speed of progression is sometimes very high, and the resulting deformation is very large, doing the scan often is required for early detection of the deformation.

The second drawback is that X-ray images only provide 2D information. The 3D deformity in scoliosis needs to be described by 3D parameters, like the rotation in the axial plane (axial rotation) and the rotation in the coronal plane (vertebral tilt). These parameters are difficult to derive from one or two 2D images. Although the vertebral tilt can be straightforwardly determined from the AP X-ray image, determining the axial rotation is difficult and gives only an estimation. The method proposed by Nash and Moe [17] estimates the axial rotation from the offset of the appearing two pedicles relative to the vertebral body. The method of Perdriolle and Vidal also uses the AP X-ray image and utilize a device called Perdriolle torsion-meter [19,25,26]. Despite the reports of its accuracy, deriving 3D information from only one 2D image is debatable and it is said to only give an “apparent rotation” [18].

Based on these drawbacks, ultrasound was selected as the imaging modality. Apart from the non-detrimental effect in clinical practice, ultrasound is also available in almost every hospital. The operation of ultrasound requires no complicated protocol, and a scan can be done in any position including standing. Such an ultrasound based system should be able to provide a 3D ultrasound image (ultrasound volume). It should also be able to accommodate the length of the human spine. The selected system that fulfils the two requirements is freehand 3D ultrasound system.

Since ultrasound imaging is often used as a non-invasive imaging technique for soft tissues [18] and it is more difficult to apply to bony structures, this paper describes a feasibility study of ultrasound system to realise a 3D ultrasound image (ultrasound volume) of large segment of human spine using a 3D freehand ultrasound system, and a framework of procedures to perform the ultrasound imaging is presented. The study was done on a volunteer that was expected has normal spine.

The structure of this paper is organized as follows. In Section 2 we explain present research in ultrasound imaging for bony structures and the types of 3D ultrasound system. The following two sections describe two separate procedures. The image acquisition is described in Section 3, while the volume reconstruction is described in Section 4. Finally, Section 5 contains the discussion and conclusions.

2. Ultrasound imaging

2.1. Ultrasound imaging for bony structure

Bony structures such as human vertebra have an acoustic impedance much higher than the surrounding material, therefore an ultrasound beam cannot penetrate it and will be reflected almost totally. Parts perpendicular to the beam direction deliver a strong signal, while the others provide a weak signal or no signal at all [3]. If the scan is performed from the back of the human body, several parts of the vertebrae such as transverse processes, laminae, and spinous processes can be captured as shown in Fig. 2 (the inverted image of an ultrasound frame).

Several results in imaging bony structure were reported in the literature. Hunerbein [9] used ultrasound to scan tissues and bone lesion, Muratore [16] focused their experiment on a vertebral phantom for the registration, and Brendel [2] performed the registration of ultrasound images of 4 lumbar vertebrae with the CT images of the same person. Scanning the large part of the spine instead of a few vertebrae as presented in this paper is more complicated. The scan time will be much longer and movement artefacts will occur. The scan must be performed in several segments and this requires an accurate volume reconstruction.

2.2. 3D ultrasound system

A 3D ultrasound system is required to fully observe an object. After scanning, this system offers further processing and examination in offline mode. The 2D slices can be viewed along 3 main view planes, and arbitrary oblique views. Finally 3D visualization can be performed. A complete review of 3D ultrasound imaging was reported in [6,7], while the history of the development of the 3D ultrasound system is described in [1].

Based on the movement of the transducers, the 3D ultrasound systems are divided into 3 major categories: mechanical 3D, 3D probe, and freehand 3D ultrasound system. The first uses a conventional 2D probe, held by a special handling mechanism and moved in a regular manner by a device such as

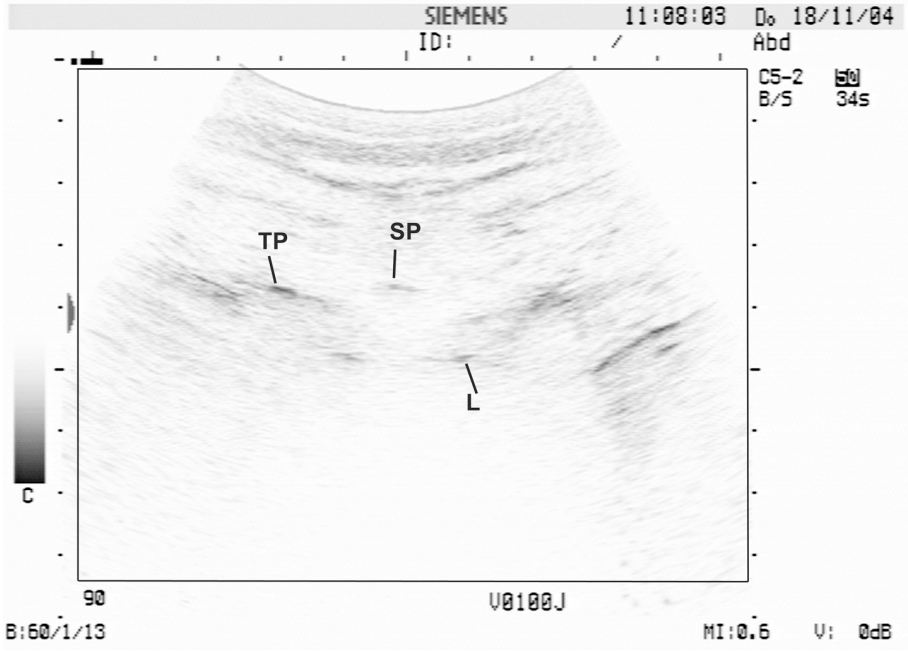

Fig. 2. The inverted image of an ultrasound frame resulting from the image acquisition procedure. It consists of the ultrasound image and other textual information. The expected vertebral parts are visible (marked by the lines) such as the transverse process (TP), spinous process (SP), and lamina (L). The same features appearing symmetrically are not marked. The region of interest which contains no textual information (inside the rectangle) was used in the next procedures.

a stepper motor. Several publications mentioned the use of this type of system [12,14]. The second type uses a special and expensive 2D phased-array probe, in which steering is done electronically. At the same time the images are obtained and stored on the computer or ultrasound machine. Although this type of 3D ultrasound system is widely used in obstetrics [20], it is also used for examining other human organs or objects having a size within the capture range of the probe [9,13,15,21,24]. The last system, also known as POM (position and orientation measurement) 3D ultrasound system, consists of a conventional 2D ultrasound machine, passive or active markers mounted on the probe and at the patient's position reference, a tracking system (optical or magnetic) to obtain the position and orientation of the marker, and a computer system (hardware and software) to manage it. Scan applications of this system are only limited by the volume that can be detected by the positioning system (tracking system).

The human spine is relatively long compared to other anatomical structures. It also has a specific morphology. Therefore, in our experiment a freehand 3D ultrasound system was a logical choice.

3. Image acquisition

In the image acquisition procedure, we used the freehand 3D ultrasound system (FH3DUS) of the Institute of High Frequency Engineering, Ruhr-University Bochum (Bochum, Germany). This system (Fig. 3) consists of a 2D ultrasound machine (Siemens Sonoline Omnia), an optical tracking system (Polaris from NDI) with active markers to determine the position of the ultrasound probe and objects in 3D space, and a computer system. The positional accuracy of the 3D ultrasound system was reported to be 0.66 mm [4]. A 5 MHz curved array probe with an imaging depth of 90 mm and a frame rate of

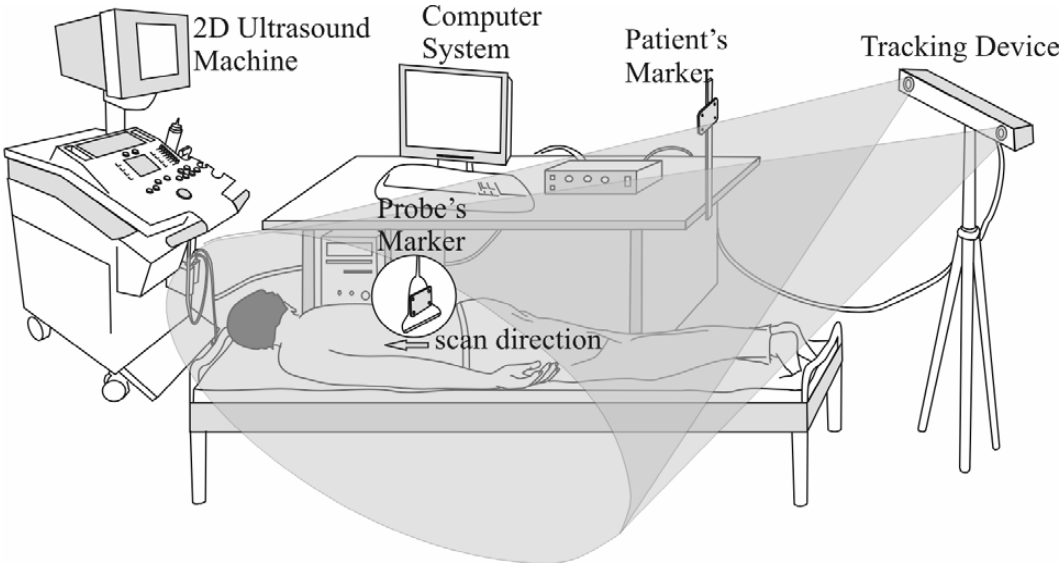

Fig. 3. A freehand 3D ultrasound system consists of a conventional 2D ultrasound machine, a tracking device with several markers, and a computer system.

34 frames per second was used. The ultrasound data was acquired via the SVHS-interface of the 2D ultrasound machine and a frame grabber card (IDS Falcon). Thus, the recorded frames contained the images as they appear on the screen of the ultrasound machine and comprise not only the ultrasound image itself, but also other textual information that must be excluded during the reconstruction procedure. A frame consisted of 800 $\times$ 600 pixels, and the frame rate of the SVHS-interface was 25 frames per second (PAL-standard). The pixel size that was obtained during the calibration process is 0.21 mm in horizontal and vertical directions.

A volunteer was lying on a bed. The ultrasound imaging plane corresponded to the transverse plane of the volunteer, and the transducer was moved freely along the spine in longitudinal direction. Due to the memory limitation of the system and the ability of the volunteer to hold his breath six scans of six overlapping volume segments of the spine were performed (Fig. 4). The overlap ensured that large part of the spine was scanned. The boundaries of the segments were marked on the volunteer's back.

During the scan in one segment, which was done in a single sweep and took on average 20 seconds, the volunteer held his breath at full inspiration. The result, as a stream of frames, was stored in one file. In total, the images of the spine were stored in six frame files. The size of a frame file does not depend on the length of the scanned area but on the scan time. Hence, the speed and the smoothness of movement of the probe were important. If the speed is too high, the gaps between scanned planes will increase, while if it is too low, the scanned area will be decreased. For a single volume segment, the lowest speed was 2.2 mm/s and the highest was 4 mm/s.

The position and orientation of the probe in 3D space obtained from the tracking system were associated with the corresponding frames and stored in the same frame file. Other information stored in the frame file were the pixel size, the centre of the image coordinate system, the transformation matrix from the image coordinate system to the probe coordinate system, and the transformation matrices of the tracking device coordinate system to the patient's reference coordinate system for all frames.

The number of frames of each frame file resulted from this procedure varied as shown in Table 1. A frame resulting from the image acquisition process is displayed in Fig. 2. The expected vertebral

Table 1
The number of frames of each frame file resulted from the ultrasound image acquisition process using a freehand 3D ultrasound system

Frame file	Number of frames
1	437
2	459
3	528
4	502
5	539
6	583

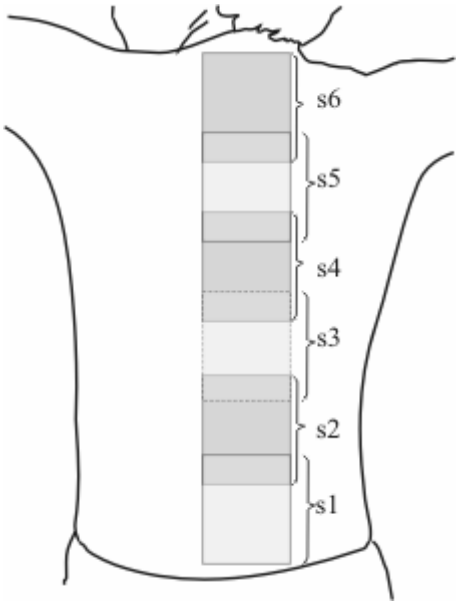

Fig. 4. Six overlapping volume segments (VS_1 until VS_6) scanned on the back of the volunteer. The scan direction is from the lower part to the upper part.

parts such as the transverse processes, spinous process, and laminae are visible. The ultrasound frame comprises not only the ultrasound image itself, but also other textual information that must be excluded during the volume reconstruction procedure.

4. Volume reconstruction

All frames achieved from the image acquisition procedure were used to create a volume of the volunteer's spine. The movement of the back of the volunteer during the scan of different segments was taken into account although the volunteer held his breath at full inspiration during the scan of the six segments. To accommodate the movement issue, in the volume reconstruction procedure, two additional sub-procedures are added to the original procedure [23]. The overall sub-procedures become: bin-filling to position the frames to a volume, hole-filling to estimate the values of missing voxels, volume segment alignment to align the six volume segments, and volume segment compounding to combine the six

volume segments into one volume. Also, a comparative study of hole-filling methods to find the best one is described.

The volume reconstruction was performed with custom software we developed for Matlab 7 (The MathWorks Inc., Massachusetts, USA) on a Pentium IV 2.8 GHz processor computer with 2 GB memory.

4.1. Bin-filling

The bin-filling procedure was utilized to position the frames from each frame file into the corresponding volume segment. Thus, segments were treated separately. The overall volume was created later on (see Section 4.4).

As mentioned in the previous section, during ultrasound image acquisition, information about 3D position and orientation of each frame was embedded to the frame, and other information such as transformation matrices was stored in the frame file. In the process, the textual information was excluded; we refer to the frame without textual information as image instead of frame. Pixels $\mathbf{w}$ in the image are transformed to location $\mathbf{u}$ within a volume by the transformation matrix $\mathbf{T}$ with the following equation

$$\mathbf{u} = \mathbf{T}\mathbf{w}, \tag{1}$$

where $\mathbf{T}$ consists of a sequence of four 4×4 homogeneous transformation matrices ${}^{V}\mathrm{T}_{P}\,{}^{P}\mathrm{T}_{R}\,{}^{R}\mathrm{T}_{S}\,{}^{S}\mathrm{T}_{I}$, $\mathbf{w}$ is a 4×1 homogeneous vector of a pixel in the image (its transpose $\mathbf{w}^{T} = [\mathrm{i\ j\ 0\ 1}]$) and $\mathbf{u}$ is a 4×1 homogeneous position vector of a voxel in the volume (its transpose $\mathbf{u}^{T} = [\mathrm{x\ y\ z\ 1}]$). The notation ${}^{S}\mathrm{T}_{I}$ means that this matrix is used to transform the I-coordinate system into the S-coordinate system. As shown in Fig. 5, I is the coordinate system used in the image, while S is the probe coordinate system (i.e. the coordinate system of the marker mounted on probe). The tracking system has its own coordinate system R, and the second marker, which was placed near the volunteer, has also its own coordinate system (P). The volume coordinate system (V) was used to index the voxels of the volume.

One of the consequences of holding the 2D ultrasound probe freely by hand is the presence of overlapping parts [23]. Voxel values of these parts were determined (compounded) based on pixel values of the intersecting images. This process is known as spatial compounding. The averaging operation was used for the compounding procedure of images since this operation is broadly used instead of finding a minimum, maximum or median value for the intersecting images [11]. The algorithm used in the bin-filling operation was described in [23]. The input of this stage was six frame files and the output was six volume segments. Therefore, we modified their algorithm as is shown in Algorithm 1. This algorithm composes of three nested loops. The outer loop is used to read the six frame files, the first inner loop is used to traverse the whole frames of a frame file, and the second inner loop is used to visit all pixels within the region of interest of each frame. In the outer loop a frame file is read. The transformation matrices of all frames, pixel size, and centre of the image coordinate system are also obtained. In the first inner loop a region of interest (ROI) of each frame is cropped. All pixels in this ROI are transformed to a volume segment in the second inner loop. Since the frames have arbitrary orientation a voxel location may be occupied by more than one pixel. Pixels occupying the same voxel location will be averaged. In doing this, a temporary variable is used to count the number of pixels that contribute to each voxel location. The results of the implementation of this algorithm are six volume segments (VS).

The image of the spine was stored in six separate VSs. An offset index was associated to each VS. The *begIm* parameter was used to store this index. The offset index in the Z-axis of the first slice of each VS was relative to the first slice of the first VS (VS1).

% Bin-filling
1. for p=1 until num_of_frame_file
2. open frames_file_F(p)
3. create volume_VS(p)
4. for q= 1 until number_of_frames_in_F(p)
5. read frame
6. crop_the_ROI_(region_of_interest)
7. for k=1 until number_of_pixels
8. transform_each_pixel_I_to_the_
volume_VS_by_
$VS = {}^{V}\mathbf{T}_{P}{}^{P}\mathbf{T}_{R}{}^{R}\mathbf{T}_{S}{}^{S}\mathbf{T}_{I}\,I$
9. if VS_{ijk}_ is_empty
10. assign I_{mn}_to_VS_{ijk}
11. else
12. assign VS_{ijk} by_
$$VS_{ijk} = \frac{c \times VS_{ijk} + Imn}{c+1}$$
(c is the number of pixels
occupied the same voxel)
13. repeat_from_7
14. repeat_from_4
15. find_and_store_the_minimum_value_of_Z_*begIm*
16. repeat_from_1

Algorithm 1. The bin-filling algorithm. In each iteration, one frame file is processed. The results are stored in a volume segment file. In the first inner loop, each frame is read and in the second inner loop all pixels within the region of interest are transformed to the volume segment.

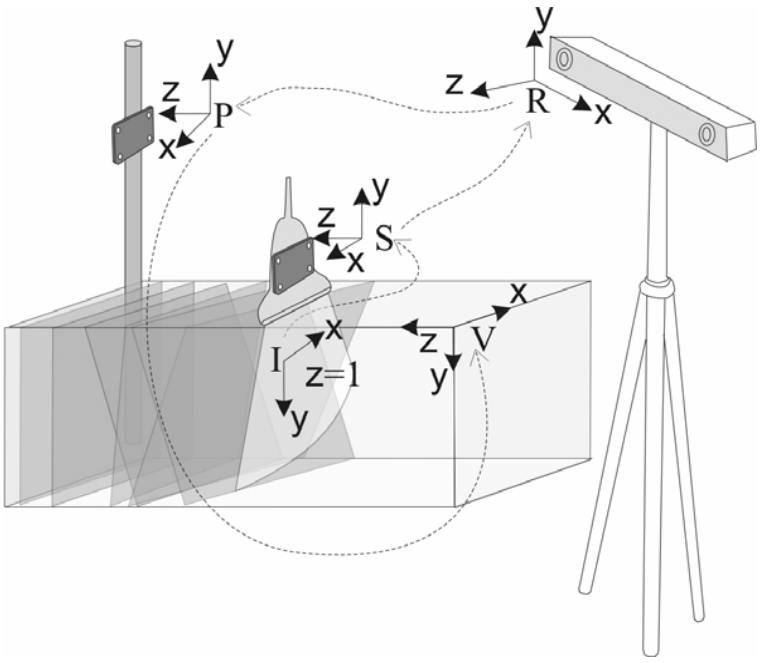

Fig. 5. In the bin-filling procedure, a pixel in the image (I) coordinate system is transformed to the probe (S) coordinate system to the tracking system (R) coordinate system to patient reference (P) coordinate system and to the volume (V) coordinate system.

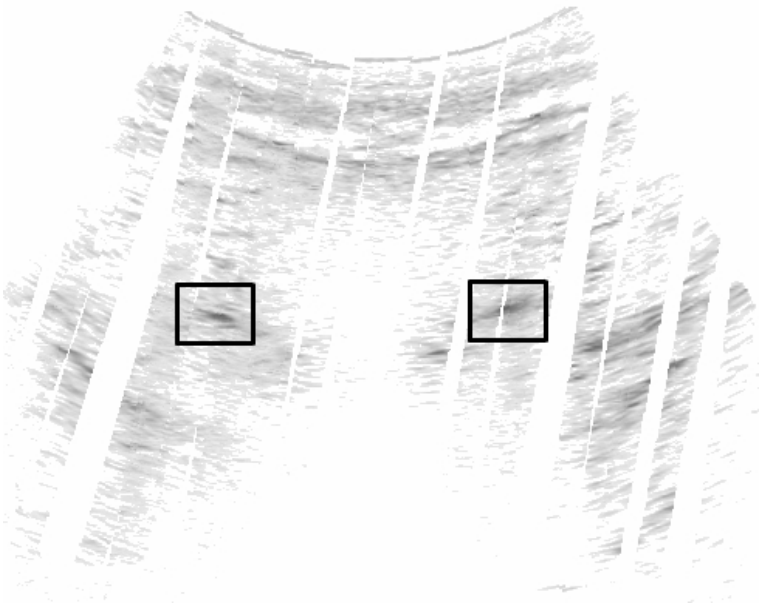

Fig. 6. Two volumes of interest (VOIs) used in the measurement of the noise level of a single measurement of the bin-filling procedure and in the comparative study of the hole-filling methods.

The size of an isotropic voxel of 0.21 mm across was used. An axial slice of the thoracic part that resulted from the bin-filling stage is shown in Fig. 8a. The expected vertebral parts (pointed by the lines) are visible. The straight form of the empty regions (white parts) was expected. They resulted from the intersection between planar surfaces (images) in 3D space.

Quantitatively, the bin-filling can be used to measure the noise level of a single measurement. The measurement was done on the volume of interest (VOI) consisting of clouds of voxels with high intensities. These clouds represent the vertebral parts. In each segment, two VOIs were defined manually around these features (Fig. 6). Then, voxels occupied by more than one scan plane were collected.

The noise level can be calculated as follows. The speckle of an ultrasound image of a human spine was assumed to follow the Gaussian distribution. The estimate mean absolute noise level (assuming Gaussian noise) is determined by the following equation

$$E_a = \frac{2}{\sqrt{\pi}}\sigma_v, \tag{2}$$

where σ_v is the estimate value of standard deviation of a single ultrasound sample. It is calculated using

$$\sigma_v = \frac{1}{M}\sum_{i=1}^{M}\sigma_i, \tag{3}$$

while M is the number of voxels intersected by two or more planes, σ_i is the standard deviation of voxel i.

The estimated value of standard deviation of a single ultrasound sample (σ_v) was found to be 9.97 calculated from 1,477,208 voxels. The estimated mean absolute noise level of a single measurement (E_a) was 11.25.

Table 2
The mean absolute grey value error of the hole-filling methods in a VOI for different percentages of missing voxels

#	Method	10%	20%	30%	40%	50%	60%
1	FPMe	11.45	11.44	11.42	11.44	11.42	11.40
2	FPMd	11.11	11.10	11.09	11.10	11.09	11.04
3	FPOl	11.20	11.18	11.17	11.18	11.16	11.13
4	VPMe	6.42	6.73	7.09	7.43	7.75	8.05
5	VPMd	6.51	6.81	7.19	7.52	7.84	8.13
6	VPOl	6.38	6.71	7.08	7.42	7.74	8.04

4.2. Hole-filling

Another consequence of holding the 2D ultrasound probe freely by hand is that parts will be missed during scanning. In the volume segments resulting from the previous stages, these parts were represented by empty voxels. The aim of the hole-filling is to estimate the values of these voxels based on the value of neighbouring voxels. In this experiment, a comparative study of several hole-filling methods as reported in the literature was performed to select the best one.

By considering the anatomical structures of a vertebra, a spherical neighbourhood was applied instead of a cubic neighbourhood. Voxels lying within a sphere of radius r will be taken into account. In the process to search the neighbouring voxels, two methods were applied, fixed radius and variable radius. In the variable radius method, the search starts using a sphere with radius $r = 1$ (voxel). If there is no filled voxel, the process continues to check voxels within a sphere with $r = 2$, and so on. Voxel size of 0.21 mm was used and the search was limited until $r = 5$ considering the size of the vertebral parts such as the spinous process. In the fixed radius method, the process only took into account voxels lying within a sphere with $r = 5$.

The ideas of the pixel nearest-neighbour (PNN) method as described in [1,22] were adopted. The average and median operation for PNN were used and the use of the *olympic* operation [8] was proposed. In the olympic operation grey values of neighbouring voxels were sorted. Then, n% of the lower values and n% of the higher values were removed. In the experiment, the value of 20 was chosen for n. The result of the olympic operation was the average of the remaining values. The PNN in combination with the variable and fixed radius, and the three operations resulted in six different PNNs (see Table 2): the fix radius PNN with average (FPAvg), median (FPMd) and olympic (FPOl), the variable radius PNN with average (VPAvg), median (VPMd) and olympic (VPOl).

The algorithm of one of the hole-filling methods, the variable PNN with Olympic operation, is shown in Algorithm 2. This algorithm is composed of three nested loops. In the outer loop every image is read. Then, empty voxels are extracted. The iterations of the empty voxels are done in the first inner loop. For each empty voxel, first, neighbouring voxels within radius $r = 1$ are checked. If non-empty voxels are found the estimated value is calculated using the Olympic operation. Otherwise, the algorithm continues to check voxels within a larger radius until $r = \text{max\_radius}$. In our experiment the max_radius was 5.

This comparative study focussed on the parts that represent vertebral features. Estimating missing values in this region, as described in the following paragraphs, is more difficult than the low contrast region. The same volume of interest (VOI) as described in Section 4.1 was used. By having the same VOIs, the results of a comparative study of this procedure can be compared with the results of the noise level of a single measurement.

We had neither a ground truth about the real grey value of each missing voxel nor the volume as a reference. Therefore, the methods were compared in the following way. Parts of the non-missing

```
%holes_filling
1. for p=1 until number_of_images
2.   read images_ Im
3.   extract_empty_voxels_ Ev
4.   if Ev<>0
5.     for q=1 until number_of_empty_voxels
6.        for r=1 until max_radius
7.          E=find_voxels_arround_Ev(q)_in_radius_r
8.          if found
9.            calculate_new_value_of_Ev(q)_by
10               Im(Ev(q))=olympic(E)
11.            exit_loop
12.       repeat_from_6
13.     repeat_from_5
14.  store images_ Im
15.repeat_from_1
```

Algorithm 2. The hole-filling algorithm. A series of images are read and empty voxels of these images are extracted. In the inner loop, the value of each empty voxel is calculated based on the neighbours lying within radius r, start from 1 until max_radius.

voxels of each VOI were selected randomly and set to zero. This process introduced holes to the dataset resulting in the new VOI with removed voxels (VOI-R). The new grey values were then estimated using the six inspected hole-filling methods to the VOI-R. The absolute grey value differences between the new and the original one of all inspected voxels were then averaged. The mean absolute grey value error adopted from [22] was formulated as

$$E_h = \frac{1}{N-1} \sum_{i=1}^{N} |p_i - q_i|. \tag{4}$$

The sum of the absolute errors is divided with $N-1$ instead of N because one degree of freedom was lost in the (implicit) calculation of the mean (Section 4.1). The variable p_i is the original grey value, q_i is the estimated grey value, and N is the number of removed voxels. For each VOI, six different values of N were chosen: 10%, 20%, 30%, 40%, 50% and 60%. A random generator function delivered 12, 12, 11, 10, 7 and 5 VOI-Rs, respectively.

The best hole-filling method was decided based on rank sum statistics. For each VOI-R, the results were ranked and the method that came out on top (the method that has the lowest mean absolute grey value error) was selected. The best method was the one that has the lowest rank sum. The statistical significance was computed using the exact permutation test on the rank sums. The best was selected to be used in the hole-filling stage for all volume segments.

The mean absolute grey value errors of different VOI-Rs of a VOI are displayed in Table 2. As can be seen, the olympic operation combined with a variable radius performs best throughout. The difference in the number of missing voxels affects only the PNN with variable radius approach, while PNN with fixed radius shows more or less the same results. The fewer missing voxels, the better the results are. The variable radius approach gives better results than the fixed radius. The olympic operation is better than the average and median operation ($p < 0.001$). The results of PNN methods with fixed radius are comparable and the results of PNN methods with variable radius are smaller in magnitude to the noise of a single measurement as discussed in Section 4.1. The best method, the PNN with variable radius and olympic operation, was used to fill empty voxels of all volume segments.

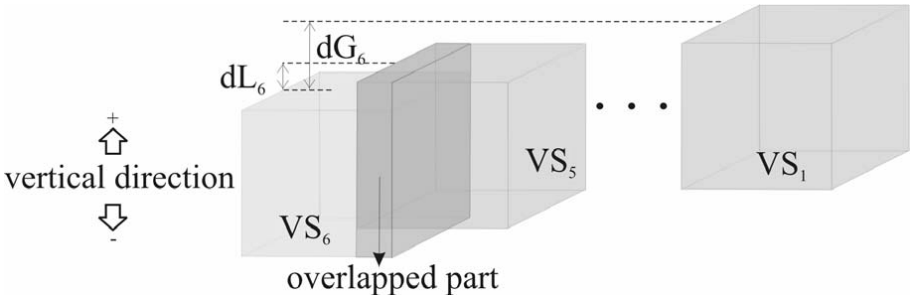

Fig. 7. Volume segment alignment procedure. Volume segment 6 (VS_6) is aligned to VS_1 using the value of dG_6.

4.3. Volume segment alignment

The goal of this stage was to align the six volume segments. In our experiment, the first VS was chosen as the reference. Although during the scanning process the volunteer was asked to hold his breath after inhaling, this procedure was mandatory to align position between two adjacent VSs. From inspection of the movement of the back of the body during breathing the shifts were assumed to be only present in the vertical direction in the prone subject. The volume segment alignment procedure is illustrated in Fig. 7. A local displacement of VS_i (dL_i) was determined by calculating the maximum value of the cross-correlation of the overlapped part between VS_i with VS_{i-1}. In this case, VS_i was aligned to VS_{i-1}that acted as a local reference. For the whole VSs, the first VS (VS_1) was used as a reference and the other five VSs (VS_2 until VS_6) were aligned to VS_1 using the global displacement value (*dG*) and was calculated using

$$dG_j = \sum_{i=2}^{j} dL_i. \tag{5}$$

The global displacement value of VS_j is equal to the cumulative local displacement of VS_2 (dL_2) until VS_j (dL_j).

The algorithm in Algorithm 3 is used to implement this stage. The first VS is used as the reference, the other five VSs are displaced based on the global displacement value (*dG*). At the beginning of the algorithm, *dG* is set to 0. In the first iteration, VS_2 and VS_1 are read. Then, the overlapping part is determined. It uses the *begIm* parameter of each VS obtained from the bin-filling stage. By associating the *begIm* to the index of each slice the overlapping slices can be determined. They are slices that have the same index value. In the next step local displacement (*dL*) of VS_2 is determined by calculating the maximum value of the cross-correlation function of these overlapping slices. The value of *dL* is used to update the cumulative global displacement value (*dG*). Afterwards, *dG* is used to update VS_2. The second iteration is done for the pair VS_2 and VS_3, and similar for the next iterations.

The results of the local and global displacement calculation of VS_2 until VS_6 are displayed in Table 3. VS_5 and VS_6 are the most misaligned. They are located outermost from the reference (VS_1) and the most movable parts during breathing in a prone position. Compared to the positional accuracy of the freehand 3D ultrasound system used in the image acquisition procedure which is reported to be 0.66 mm, the *dG*s values are larger at certain ranges. Therefore, the volume segment alignment is necessary.

Table 3
The displacement values of each volume segment (VS)

VS	Local displacement (dL) in mm	Global displacement (dG) in mm
VS2	0.83	0.83
VS3	−0.85	−0.02
VS4	0.01	−0.01
VS5	−2.63	−2.64
VS6	−3.60	−6.24

```
% volume_segments_alignment
1. dG = 0
2. for p=2 until num_of_volumes
3.    open volume_VS(p-1)
4.    open volume_ VS(p)
5.    find the_overlapped_part_of_VS(p-1)_and_VS(p)
6.    find the_local_displacement_dL
7.    dG = dG+dL
8.    update volume_VS (p)_with_dG
9. repeat_from_2
```

Algorithm 3. The volume segment alignment algorithm. In each iteration, two adjacent volume segments are opened. The overlapping part is determined from these volume segments, then the local displacement (*dL*) is calculated using cross correlation function. The second volume segment is updated using global displacement value (*dG*).

```
% volume_segments_compounding
1. for p=1 until num_of_volumes
2.    open volume_VS(p)
3.    for q= 1 until number_of_slice_in_VS(p)
4.      iIm = begIm+q-1
5.      read slice(q)_Sq
6.      if no_image_correspond_to_ iIm
7.         create image_file_imCurr
8.      else
9.        open image_file_imCurr
10.    update imCurr_with_ Sq
11.  repeat_from_3
12.repeat_from_1
```

Algorithm 4. The volume segments compounding algorithm. In the inner loop, a slice is read and stored to an image if the image corresponding to **iIm** does not exist. Otherwise, the image is read and updated using the current slice. **iIm** depend on the value of *begIm* that is previously obtained during the bin-filling process.

4.4. Volume segment compounding

The volume segment compounding was required to combine the six volume segments into one volume. The scans had been performed in such a way that there was an overlapping part between two adjacent volume segments. In this sub-procedure, the value of the overlapping part was the average value of the values of the two segments. Algorithm 4 was used to implement this purpose.

The result of this stage was a volume that was stored as a sequence of images. The index of an image in the Z-axis was associated with its name. The *begIm* parameter obtained in the bin-filling procedure was used. The algorithm is composed with two nested loops. The outer loop is used to read the six VSs. In each iteration of this loop, the inner loop is called to read a slice of index q of the VS. The new

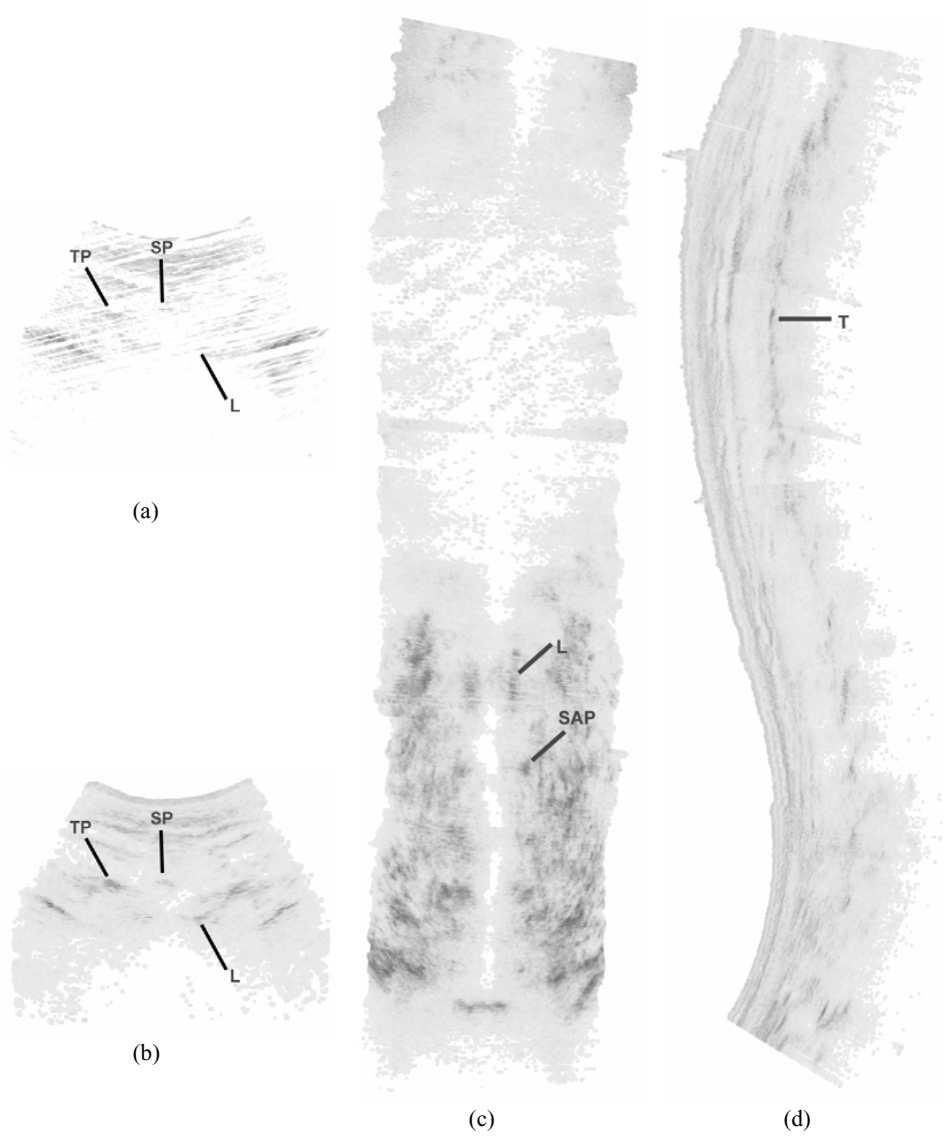

Fig. 8. (a) An axial slice of the thoracic part resulting from the bin-filling sub-procedures. The slices of the volume resulted from the volume reconstruction: (b) the corresponding slice of (a), (c) coronal slice and (d) sagittal slice. The expected vertebral parts are visible (marked by the lines) such as the transverse process (TP), lamina (L), spinous process (SP), or superior articular process (SAP). The same features appear symmetrically are not marked.

index *iIm* is determined from $begIm+q-1$. The image file corresponding to the *iIm* is then checked. If no image file is associated with this index this slice is stored as an image that includes *iIm* in its name. Otherwise, the image is read and updated by the current slice using the average operation. The current slice is shifted over an integer number of pixels found by rounding off *dG*.

The output images of this sub-procedure represent the resulted volume. The number of images is 2374. The image size is 622x772 pixels. The complete scanned spine of the volunteer has the length of 498.5 mm (with the isotropic voxel of 0.21 mm). Axial, coronal and sagittal slices of the results are

shown in Fig. 8b, c and d respectively. Some of the vertebral parts are indicated by the lines.

5. Discussion and conclusions

We have described a framework that can be used for imaging a large part of human spine using a freehand 3D ultrasound system. The overall results show that the procedure is feasible. The framework consisted of an image acquisition procedure followed by a sequence of sub-procedures of volume reconstruction: bin-filling, hole-filling, volume segment alignment, and volume segment compounding.

In the ultrasound image acquisition procedure, the freehand 3D ultrasound system is an appropriate system to be used since it could cover the spine and offers sufficient flexibility to follow the spinal morphology. By limiting the length of a scan segment the scan time is limited as well and thus movement artefacts caused by breathing can be reduced. On the other hand, scanning the large spine in a limited number of segments is beneficial. It will decrease the possibility of shift or misalignment between the overlapping segments and also shorten the time of each scan. The spine was scanned in six segments, a compromise between small overlap errors and small movement errors.

The volunteer was scanned in a lying position to obtain good images despite in the common protocol, bi-planar radiographs are taken from a scoliotic patient in a standing position. This position was chosen since a device that can maintain the standing position of the volunteer was not available yet. With such a device it will be possible to scan a person in the preferred upright position.

In the volume reconstruction procedure, the sequence of stages resulted in fairly good images. The expected vertebral features, such as the transverse processes, laminae, superior articular processes, and spinous process, appeared. In a sagittal slice, a string of transverse processes appeared representing the curvature of the spine. They are comparable to the ultrasound images shown in [3,16]. The appearance of the vertebral features is necessary to enable determination of the position and orientation of each vertebra in 3D space and the curvature of the spine.

In the hole-filling stage many methods are mentioned in the literature and they are mainly applied for non-bony structures. In our application that includes bony structures, only simple and fast method like the pixel nearest-neighbour (PNN) was inspected. The PNN in combination with the variable and fixed radius, and the three operations: mean (average), median and the newly proposed *olympic* operation, resulted in six different PNNs. The results of our comparative study of the hole-filling methods show that the PNN method is suitable to be used. The olympic operation is better than the mean and median operations. In practice the differences among them are small. The variable radius approach gives better results than the fixed radius approach. The best method among the six inspected methods is the PNN with variable approach and olympic operation. It has the lowest rank sum in the rank sum statistics. Compared to the noise of a single measurement, in magnitude the results of the PNN methods with fix radius approach are comparable and the PNN methods with variable radius approach were far less. They were also comparable to the results in [11,22], therefore there is no immediate need to investigate other methods.

Volume segment alignment is necessary since in our experiment the displacement values of volume segments are higher than the positional accuracy of the 3D ultrasound system that was used in the image acquisition procedure.

The speed of the volume reconstruction procedure, which took a day for the presented method, was not considered to be a great issue yet. We first wanted to prove that a freehand 3D ultrasound system is feasible for imaging the human spine. In clinical application the speed is important since the physician and the patient need the result just after the scanning process to verify whether the scan should be redone

or not. Optimization of the algorithm, C++ implementation, the specification of the computer including the number of processors it has, and the relocation of the computation tasks to the GPU (graphics processing unit) are expected to give much faster results.

Acknowledgements

The authors acknowledge the support of the Institute of High Frequency Engineering, Ruhr-University Bochum, Germany, for using their freehand 3D ultrasound system. Their valuable information and great help is appreciated. We also would like to express our gratitude to Jan Visscher (Department of Radiology, University Medical Center Groningen, University of Groningen, The Netherlands) for his support in preliminary ultrasound experiments.

References

[1] C.D. Barry, C.P. Allott, N.W. John, P.M. Mellor, P.A. Arundel, D.S. Thomson and J.C. Waterton, Three-dimensional freehand ultrasound: Image reconstruction and volume analysis, *Ultrasound in Medicine & Biology* **23** (1997), 1209–1224.
[2] B. Brendel, S. Winter, A. Rick, M. Stockheim and H. Ermert, Bone registration with 3D CT and ultrasound data sets, *International Congress Series* **1256** (2003), 426–432.
[3] B. Brendel, S. Winter, A. Rick, M. Stockheim and H. Ermert, Registration of 3D CT and ultrasound datasets of the spine, *Computer Aided Surgery* **7** (2002), 146–155.
[4] B. Brendel, S. Winter and H. Ermert, A simple and accurate calibration method for 3D freehand ultrasound, unpulblised.
[5] M.M. Doody, J.E. Lonstein, M. Stovall, D.G. Hacker, N. Luckyanov and C.E. Land, Breast cancer mortality after diagnostic radiography – findings from the us scoliosis cohort study, *Spine* **25** (2000), 2052–2063.
[6] A. Fenster and D.B. Downey, Three-dimensional ultrasound imaging, *Annual Review of Biomedical Engineering* **2** (2000), 457–475.
[7] A. Fenster, D.B. Downey and H.N. Cardinal, Three-dimensional ultrasound imaging, *Physics in Medicine and Biology* **46** (2001), R67–R99.
[8] R.C. Gonzalez and R.E. Woods, *Digital Image Processing*, Addison-Wesley Pub, 1992.
[9] H. Hünerbein, M. Raschke, C. Khodadadyan, P. Hohenberger, N.P. Haas and P.M. Schlag, Three-dimensional ultrasonography of bone and soft tissue lesions, *European Journal of Ultrasound* **13** (2001), 17–23.
[10] J. Hecquet, J. Legaye and G. Duval-Beaupere, Access to a three-dimensional measure of vertebral axial rotation, *Eur Spine J* **7** (1998), 206–211.
[11] R.S. Jose-Estepar, M. Martin-Fernandez, P.P. Caballero-Martinez, C. Alberola-Lopez and J. Ruiz-Alzola, A theoretical framework to three-dimensional ultrasound reconstruction from irregularly sampled data, *Ultrasound in Medicine & Biology* **29** (2003), 263–277.
[12] J.F. Krücker, C.R. Meyer, G.L. LeCarpentier, J.B. Fowlkes and P.L. Carson, 3D spatial compounding of ultrasound images using image-based nonrigid registration, *Ultrasound in Medicine & Biology* **26** (2000), 1475–1488.
[13] F. Lefebvre, N. Graillat, E. Cherin, G. Berger and A. Saied, Automatic three-dimensional reconstruction and characterization of articular cartilage from high-resolution ultrasound acquisitions, *Ultrasound in Medicine and Biology* **24** (1998), 1369–1381.
[14] D.F. Leotta and R.W. Martin, Three-dimensional spatial compounding of ultrasound scans with weighting by incidence angle, *Ultrasonic Imaging* **22** (2000), 1–19.
[15] S.S. Mehta, A.R. Azzouzi and F.C. Hamdy, Three dimensional ultrasound and prostate cancer, *World Journal of Urology* **22** (2004), 339–345.
[16] D.M. Muratore, J.H. Russ, B.M. Dawant and R.L. Galloway, Three-Dimensional Image Registration of Phantom Vertebrae for Image-Guided Surgery: *A Preliminary Study* **7** (2002), 342–352.
[17] C.L. Nash, Jr. and J.H. Moe, A study of vertebral rotation, *J Bone Joint Surg Am* **51** (1969), 223–229.
[18] T.R. Nelson and D.H. Pretorius, Three-dimensional ultrasound imaging, *Ultrasound in Medicine and Biology* **24** (1998), 1243–1270.
[19] H. Omeroglu, O. Ozekin and A. Bicimoglu, Measurement of vertebral rotation in idiopathic scoliosis using the perdriolle torsionmeter: a clinical study on intraobserver and interobserver error, *Eur Spine J* **5** (1996), 167–171.

[20] M. Riccabona, D.H. Pretorius, T.R. Nelson, D. Johnson and N.E. Budorick, Three-dimensional ultrasound: Display modalities in obstetrics, *Journal of Clinical Ultrasound* **25** (1997), 157–167.
[21] M. Riccabona, Pediatric three-dimensional ultrasound: basics and potential clinical value, *Clinical Imaging* **29** (2005), 1–5.
[22] R. Rohling, A. Gee and L. Berman, A comparison of freehand three-dimensional ultrasound reconstruction techniques, *Medical Image Analysis* **3** (1999), 339–359.
[23] R. Rohling, A. Gee and L. Berman, Three-dimensional spatial compounding of ultrasound images, *Medical Image Analysis* **1** (1997), 177–193.
[24] S. Tong, D.B. Downey, H.N. Cardinal and A. Fenster, A three-dimensional ultrasound prostate imaging system, *Ultrasound in Medicine and Biology* **22** (1996), 735–746.
[25] H.R. Weiss, Measurement of vertebral rotation: Perdriolle versus raimondi, *Eur Spine J* **4** (1995), 34–38.
[26] M. Yazici, E.R. Acaroglu, A. Alanay, V. Deviren, A. Cila and A. Surat, Measurement of vertebral rotation in standing versus supine position in adolescent idiopathic scoliosis, *J Pediatr Orthop* **21** (2001), 252–256.